



HAL
open science

From amorphous to microcrystalline silicon: moving from one to the other by halogenated silicon plasma chemistry

Giovanni Bruno, Pio Capezzuto, Maria M Giangregorio, Maria Losurdo

► **To cite this version:**

Giovanni Bruno, Pio Capezzuto, Maria M Giangregorio, Maria Losurdo. From amorphous to microcrystalline silicon: moving from one to the other by halogenated silicon plasma chemistry. *Philosophical Magazine*, 2009, 89 (28-30), pp.2469-2489. 10.1080/14786430903070928 . hal-00519091

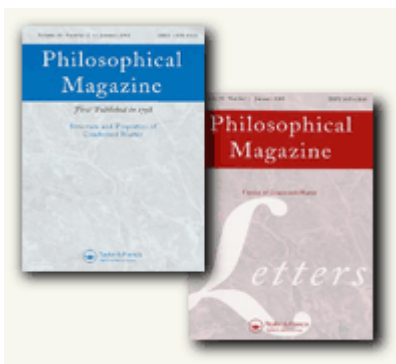
HAL Id: hal-00519091

<https://hal.science/hal-00519091>

Submitted on 18 Sep 2010

HAL is a multi-disciplinary open access archive for the deposit and dissemination of scientific research documents, whether they are published or not. The documents may come from teaching and research institutions in France or abroad, or from public or private research centers.

L'archive ouverte pluridisciplinaire **HAL**, est destinée au dépôt et à la diffusion de documents scientifiques de niveau recherche, publiés ou non, émanant des établissements d'enseignement et de recherche français ou étrangers, des laboratoires publics ou privés.



From amorphous to microcrystalline silicon: moving from one to the other by halogenated silicon plasma chemistry

| | |
|-------------------------------|----------------------------------------------------------------------------------------------------------------------------------------------------------------------------------------|
| Journal: | <i>Philosophical Magazine & Philosophical Magazine Letters</i> |
| Manuscript ID: | TPHM-08-Oct-0370.R2 |
| Journal Selection: | Philosophical Magazine |
| Date Submitted by the Author: | 20-May-2009 |
| Complete List of Authors: | Bruno, Giovanni; CNR-IMIP, Plasmachemistry Capezzuto, Pio; CNR-IMIP, Plasmachemistry Giangregorio, Maria; CNR-IMIP, Plasmachemistry Losurdo, Maria; CNR-IMIP, Plasmachemistry |
| Keywords: | a-Si:H, ellipsometry, grain growth, growth processes, interfacial structures, microcrystalline silicon, nanocrystals, plasma processing |
| Keywords (user supplied): | a-Si:H, ellipsometry, grain growth |
| | |



1
2
3 **From amorphous to microcrystalline silicon: moving from one to the other by halogenated**
4 **silicon plasma chemistry**
5
6
7

8 Giovanni Bruno,* Pio Capezzuto, Maria M. Giangregorio and Maria Losurdo
9

10
11 *Institute of Inorganic Methodologies and of Plasmas, IMIP-CNR, via Orabona 4, 70126 Bari, Italy*
12
13
14

15
16
17 **Abstract**
18

19 Amorphous and microcrystalline silicon thin films have been deposited on a large variety of
20 substrates including crystalline silicon, Corning glass and polyimide exploiting SiF₄-H₂-He
21 radiofrequency (13.56 MHz) plasma enhanced chemical vapor deposition. Spectroscopic
22 ellipsometry has been mainly applied to investigate the optical and structural characteristics of the
23 deposited films and to investigate the microstructure depending on the experimental parameters,
24 including the H₂ and He dilution of plasmas, the deposition temperature, and the substrate plasma
25 treatment prior to deposition. The film growth dynamics has also been investigated by analyzing
26 films with different thickness. The peculiarities of the SiF₄ chemistry involved in heterogeneous
27 processes during film deposition and responsible for the amorphous to micro-crystalline transition
28 are presented. It is demonstrated that the SiF₄-H₂ chemistry leads to tailoring of film microstructure
29 from amorphous to fully and dense microcrystalline silicon films without any amorphous
30 incubation layer also at temperature as low as 100°C on any substrate, including Corning glass 7059
31 and polyimide, independently of film thickness. These results and peculiarities of SiF₄-based
32 plasmas are discussed in the frame of the literature debate on SiH₄ vs SiF₄ as silicon precursor.
33
34
35
36
37
38
39
40
41
42
43
44
45
46
47
48

49 Corresponding author: tel. +39-0805442094; fax: +39-0805443562;
50

51 e-mail: giovanni.bruno@ba.imip.cnr.it
52
53
54
55
56
57
58
59
60

1. Introduction

Silicon in its different structural forms is the most widely used and investigated element in various modern technological fields and in near future nanotechnology applications. Silicon thin film have gained growing acceptance as a material from which to fabricate electronic devices such as photovoltaic cells, photoresponsive and photoconductive devices, transistors, diodes, integrated circuits, memory arrays, sensors and the like. This is because silicon thin films can be manufactured in various microstructural forms going from amorphous (a-Si) to nanocrystalline (nc-Si), microcrystalline ($\mu\text{c-Si}$) and polycrystalline (pc-Si) with a wide range of controllable electrical and optical properties. Silicon can alloy other elements (C, Ge, N, O, ...), yielding a large variety of materials with a band gap ranging from 0.7 eV to 9 eV, which can be deposited over relatively large area substrates at relatively low cost. Thus, the sentence "Earth - silicon planet" is fully justified.

The first report of amorphous silicon solar cells in 1976 [1] sparked worldwide interest in a-Si:H for its use as a viable source of renewable energy.

The discovery of the importance of hydrogen in hydrogenated amorphous silicon, a-Si:H, [2] led to a wide range of deposition conditions, which attempted to improve its properties. The early discovery of light induced changes, i.e., *the Staebler-Wronski effect*, [3,4] had a major impact on the design of the a-Si:H solar cells.

In 1981 Walter Spear [5,6], to whom this volume is dedicated, and many other groups started to investigate extensively the electronic and optical properties of microcrystalline films prepared by plasmas [7-10]. Those studies led, about ten years later, to $\mu\text{c-Si/a-Si:H}$ p-n junction solar cells with improved properties [11,12]. In 1994, the preparation of a fully microcrystalline ($\mu\text{c-Si:H}$) silicon p-i-n single-junction solar cell with new striking advantages compared to amorphous silicon (a-Si:H) was achieved [13]. The main reason driving the transition from a-Si to $\mu\text{c-Si:H}$ was the fact that the latter showed no light induced degradation unlike a-Si:H. Because of the favorable combination of the improved photostability, higher carrier mobility and lower optical absorption, $\mu\text{c-Si}$ films are being used not only for solar cells but also as carrier injection layers in thin film transistors.

The *life-motif* of improving stability against photodegradation of a-Si:H led researchers to demonstrate recently that "protocrystalline Si", produced near the amorphous-to-microcrystalline silicon transition regime, exhibits a higher degree of ordering with increased stability under light illumination [14-19].

In addition to solar cells, nanocrystalline silicon (nc-Si) because of band gap widening, photoluminescence and electroluminescence has promise applications in quantum optics and electronics [20,21].

1
2
3 Although SiH₄ is the main precursor used for the plasma enhanced chemical vapor
4 deposition (PECVD) of silicon films from amorphous to microcrystalline with [15-17,22-26] or
5 without H₂ dilution [27-34], in the course of years various halogenated Si gas precursors, e.g. SiF₄
6 [35-40], SiCl₄ [41-43], and SiH₂Cl₂ [44,45] have also been investigated and reported.
7
8

9
10 In 1978, soon after the demonstration of the hydrogen related instability in a-Si:H, a paper
11 by Ovshinsky and Madan appeared on Nature [46] reporting that “*the new Si-F-H alloys (fabricated*
12 *from the gas ratio of SiF₄/H₂=10/1) is superior to SiH₄-based film for electronic applications*”. A
13 higher mobility and a much lower density of states were reported for films grown by SiF₄ when
14 compared to SiH₄. This was the first paper opening a debate about using SiF₄ [47] as Si-precursor.
15
16

17
18 As also disclosed in U.S. Pat. No. 4,226,898 of Ovshinsky, fluorine introduced into the silicon alloy
19 semiconductor layers operates to substantially reduce the density of the localized defect states in the
20 energy gap thereof and facilitates the addition of other alloying materials, such as carbon [48] and
21 germanium [39]. As a result of introducing fluorine into the host matrix of the silicon network, the
22 produced film can have a number of favorable attributes such as high photoconductivity, increased
23 charge carrier mobility, increased diffusion length of charge carriers and low dark intrinsic
24 electrical conductivity.
25
26

27
28 In 1980, Madan and Ovshinsky also reported the doping of a-Si:F:H materials demonstrating
29 suitability for photovoltaic applications [49]. Those results were corroborated by other groups, who
30 reported a considerable smaller Staebler-Wronski effect in a-Si:H:F solar cells than a-Si:H [50,51]
31 and an improved fill factor after light soaking for cells from a-Si:F:H [52]. From the fundamental
32 point of view, Lucovsky investigated the bonding of fluorine in silicon [53].
33

34
35 In 1991, Walter Spear, after 15 years from demonstration of a-Si doping [54], also started
36 investigating the silicon deposition using SiF₄, coming to the conclusion that “*any preparation*
37 *method which allows a systematic decrease in hydrogen content without appreciable affecting the*
38 *electronic quality and Fermi level position, should improve the stability of the material with respect*
39 *to light degradation*” [55]. This citation from Spear sums up the main problem/limit of a-Si:H thin
40 films from hydrogenated systems and re-opened the debate about the SiH₄ or the SiF₄ as precursor
41 for silicon in PECVD.
42

43
44 Various aspects were underpinned by Spear [55] concerning the silicon deposition from SiF₄
45 plasmas, and are listed as follow:
46
47

48
49 - the SiF₄-H₂ system produces an efficiency-mobility-lifetime product $\eta\mu\tau$ of $10^{-5} \text{ cm}^2\text{V}^{-1}$ (the
50 product $\mu\tau$ represents the drift range per unit field of the carrier during its life time τ , and η
51
52
53
54
55
56
57
58
59
60

1
2
3 represents the efficiency of excited carrier generation). The optimum $\eta\mu\tau$ corresponds to a gas
4 residence time in the plasma reactor of 140ms, possibly representing the optimum lifetime of the
5 film growth precursor (which our group has identified being the SiF_2 radical [56]);
6
7

8
9
10 - a transition from amorphous-to-microcrystalline silicon occurs using $\text{SiF}_4\text{-H}_2$ plasmas, and it can
11 be tailored non only by the H_2 dilution but also by changing the pressure and the temperature
12 [40,55,56];
13

14
15
16 -the SiF_4 and H_2 gases have to be allowed to interact in the plasma; the atomic hydrogen itself is not
17 enough to assist dissociation of SiF_4 [54,55];
18

19
20 -the Ar^* metastable (which has a life time of 40-50s) is not capable of dissociating SiF_4 [54,55], and
21 it is necessary to avoid ion bombardment that induces disorder/amorphization, when moving to
22 microcrystalline phases.
23
24

25
26 Therefore, pioneering works from Spear, Ovshinsky and Madan posed the question: *why moving to*
27 *SiF_4 ?*
28

29
30
31 This contribution presents and discusses various aspects related to the fluorine chemistry
32 involved in the PECVD exploiting SiF_4 -based plasmas for the deposition of silicon films with
33 various microstructures. Although hydrogen atoms play a key role also in the $\text{SiF}_4\text{-H}_2$ plasmas, the
34 concomitant role of fluorine atoms and SiF_x species in the deposition process as well as in the
35 resulting films characteristics is presented.
36
37
38

39
40 Some answers to the question "*why moving to SiF_4 ?*" we have found are: (i) the capability of
41 reducing the hydrogen content in silicon films by the interaction of fluorine atoms with hydrogen
42 during silicon film deposition; (ii) the capability of determining the amorphous-to-microcrystalline
43 transition at low temperatures; (iii) the possibility of tailoring the film microstructure and texture in
44 a low hydrogen environment [57].
45
46
47
48
49
50
51
52

53 2. Experimental Approach

54
55 Si films with different microstructure ranging from amorphous (a-Si:H,F) to microcrystalline
56 ($\mu\text{c-Si:H,F}$) and with a thickness in the range 20-500 nm were deposited by a typical parallel-plate
57 r.f. 13.56 MHz PECVD using $\text{SiF}_4\text{-H}_2$ plasmas. Depositions were run at 0.3 Torr and at a r.f. power
58 density (RFPD) of 170 mW/cm^2 . The deposition temperature was investigated in the range 60°C -
59 230°C . In order to change the microstructure, the SiF_4/H_2 ratio was changed in the range 2-10. He
60

1
2
3 dilution was operated by adjusting the He flux in the range 0-100 sccm. In order to assess the
4 peculiarities of SiF₄-based plasmas, a comparison with PECVD processes using SiH₄-H₂ was also
5 carried out at gas flow rates of SiH₄-H₂=1-10 and SiH₄-H₂=0.5-30 sccm for depositing amorphous
6 and microcrystalline films, respectively. Various substrates including c-Si(100), Corning glass 7059
7 and flexible polyimide were used in our investigation.
8
9

10
11
12
13 Our approach consisted in monitoring in real time the deposition process by laser reflectance
14 interferometry (LRI) using a He-Ne laser. An extensive characterization of the films structure was
15 carried out by using X-ray diffraction (XRD), Raman spectroscopy, and by UV-visible
16 spectroscopic ellipsometry (SE). SE spectra of the real, $\langle \epsilon_1 \rangle$, and imaginary, $\langle \epsilon_2 \rangle$, parts of the
17 pseudodielectric function, $\langle \epsilon \rangle = \langle \epsilon_1 \rangle + i \langle \epsilon_2 \rangle$, were acquired with a phase modulated spectroscopic
18 ellipsometer (UVISEL-Jobin Yvon) in the range 1.5 – 6.5 eV. SE spectra of amorphous and
19 nanocrystalline films were parameterized using the Tauc-Lorentz dispersion equation [58].
20 Microcrystalline films were analyzed using the Bruggeman effective medium approximation
21 (BEMA) assuming that μ c-Si films consist of microcrystalline, amorphous silicon and voids,
22 according to the approach reported in ref. [59]. The dielectric functions of poly-Si with fine and
23 large grains from reference [60] were used, thereafter denoted as ‘p-Si-l’ (large grains) and ‘p-Si-
24 f’ (fine grains) in the models. Surface morphology was observed by atomic force microscopy
25 (AFM) in the intermittent contact mode (IC-AFM).
26
27
28
29
30
31
32
33
34
35
36
37
38
39
40
41

42 **3. Relationship occurring between the halogenated (fluorine) plasma chemistry and the** 43 **silicon nano- and microstructural transformation** 44 45

46 Despite the differences between SiF₄-H₂ and SiH₄-H₂ plasmas, many studies have indicated
47 that hydrogen plays the key-role in both plasmas. Indeed, in SiH₄-H₂ plasmas, H₂ is not
48 indispensable for the deposition of silicon films, since the good dissociation of SiH₄ provides both
49 the film growth precursors SiH_x (x=2,3) [61] and the H-atoms for tailoring film [27-34]. However,
50 all the above cited works deposited microcrystalline silicon at T>230°C. Nevertheless, H₂, i.e., the
51 hydrogen-dilution ratio R (H₂/SiH₄), has been reported by other groups to be important for aiding
52 the amorphous-to-microcrystalline silicon phase transitions [15,17,22-26], defects [62,63] and
53 electronic properties [64-68].
54
55
56
57
58
59
60

The main characteristics of halogenated, e.g. SiF₄, SiCl₄, plasmas can be summarized as follow.

3.1. Role of hydrogen in SiF₄ plasmas

The deposition of all silicon phases by SiF₄ plasmas requires H₂, as already pointed out by Spear [55]; silicon deposition from SiF₄ plasmas, which are known to be etchant, does not occur without H₂. Our group has previously demonstrated [38,69] that silicon deposition depends not only on the concentration of SiF_x species but also on H-atoms, i.e., growth rate $r_g = k[\text{SiF}_2][\text{H}]$. There are other reports [70,71] that demonstrate that the major growth precursors in SiF₄-based systems are SiH_nF_m (n+m≤3).

Due to the diffusion of SiF_x on the surface and consequently encountering with other species, a larger and more stable cluster can be formed. The cluster may finally reach a final critical size, beyond the condition that it is unlikely to desorb, creating a stable Si–Si network. During these processes, the effective etching of weakly adsorbed bonds by hydrogen and fluorine atoms can establish the crystalline structure. Although various mechanisms have been proposed to contribute to the amorphous-to-microcrystalline transition [65,72,73], the fluorine-atoms etching contributes mainly to the nano- and micro-crystallinity in SiF₄-based plasmas [74]. We have previously demonstrated a semi-quantitative correlation between the film crystallinity and the deposition/etching competition [38], which is sketched in Fig. 1.

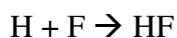
3.2 Amorphous to microcrystalline silicon transition

Differently from SiH₄-H₂ plasmas where H₂%>90% is used to deposit microcrystalline films [15,17,22-26], the a-Si to μc-Si transition in SiF₄-based plasmas does not require a high H₂ dilution, as demonstrated by various papers. As an example, Shimizu and his group have reported [75] almost complete (400)-oriented μc-Si:H,F growth at gas flow ratios of SiF₄/H₂ = 60/3 sccm at 300°C and 30 /14 sccm at 200°C, while at smaller SiF₄/H₂ gas flow ratios such as 30/10 sccm, (220)-oriented μc-Si:H,F films were obtained using very high frequency (VHF: 100MHz). Another study [76] also demonstrated that, although a high hydrogen coverage over the growing surface was necessary to obtain a large grain, a low H coverage on the growing surface could be more effective in increasing the crystalline fraction and the degree of preferential orientation of μc-Si:H,F films. We have also investigated the effect of the SiF₄/H₂ ratio on the cristallinity of μc-Si:H,F films deposited at 13.56 MHz, at low r.f. power (10 W) and at 250°C on Corning glass 7059 [39], and data are shown in Fig. 2.

Furthermore, the a-Si to μc-Si transition in SiF₄ plasmas depends also on F-atoms; and this is quite obvious to think about since it is well known that F-atoms are better etchant than H-atoms for silicon [77]. Indeed, various heterogeneous processes involve F-atoms that act not only on Si-atoms



but also on H-atoms, acting as scavenger of hydrogen atoms through the heterogeneous process



Both processes determine the amorphous-to-microcrystalline transition and the hydrogen content into the films.

Considering the bond energies involved in the system, e.g. $E(\text{H-F}) = 5.8$ eV, $E(\text{Si-F}) = 5.6$ eV, $E(\text{Si-H}) = 3.1$ eV and $E(\text{Si-Si}) = 1.8$ eV, the surface concentration of F-atoms that reach the growing surface and etch the weak Si-Si bonds is, in addition to H-atoms, an important factor in the amorphous-to-microcrystalline transition. Indeed, the formation of H-F bonds as the more favorable bond is the effective parameter for the control of the density of both F-atoms and H-atoms at the growing surface. Thus, the desorption of HF, which is completely dissociated in the plasma phase, from the film surface and the propagation of the Si-Si network explain the higher packing density, better structural and lower hydrogen content of films from SiF_4 , as found by the ellipsometric spectra analysis shown in Fig. 3. In particular, the higher density volume fraction is seen in the higher amplitude spectrum for the films obtained by SiF_4 plasmas and in the lower voids volume fraction as determined by the BEMA modeling. Furthermore, in the case of $\mu\text{c-Si:H:F}$, a good fit to SE spectra is obtained by a two-layer model including an homogeneous and dense microcrystalline layer with a thin layer of surface roughness, as also supported by AFM data. Conversely, the lower spectrum with less pronounced crystalline silicon interband critical points E_1 and E_2 recorded for $\mu\text{c-Si:H}$ from SiH_4 is indicative of a higher voids volume fraction and higher surface roughness. The best-fit model indicated a non-homogeneous multilayer structure with a voids density increasing toward the film surface.

3.3 Crystallinity at low temperature

The etching/deposition competition contributes to microcrystallinity in $\text{SiH}_4\text{-H}_2$ plasmas as well as in $\text{SiF}_4\text{-H}_2$ plasmas, where the etchant species are both atomic hydrogen and fluorine. Interestingly, a study of the temperature dependence of the etching rate of both a-Si and $\mu\text{c-Si}$ films by hydrogen atoms (produced by a H_2 plasma) and fluorine atoms (produced by a NF_3 plasma) revealed that the etching of a-Si and $\mu\text{c-Si}$ by fluorine atoms has a positive pseudo-activation energy, E_a , of +0.028 eV and of +0.11 eV, respectively, (see the like-Arrhenius plot of Fig. 4). Thus, the lower the temperature, the faster the etching of the a-Si phase than the etching of the $\mu\text{c-Si}$ phase by F-atoms. In contrast, a negative pseudo-activation energy of -0.026 eV and of -0.097 eV is found for the

1
2
3 etching by H-atoms of a-Si and $\mu\text{c-Si}$, respectively, indicating that the higher the temperature, the
4 faster the etching of the a-Si with respect to the $\mu\text{c-Si}$ phase. We have defined the ratio of the a-Si
5 to $\mu\text{c-Si}$ etching rate, $r_{\text{a-Si}}/r_{\mu\text{c-Si}}$, as an “etching selectivity” parameter. This ratio is plotted as a
6 function of temperature in Fig. 5. The plot shows that the etching selectivity in favor of the
7 microcrystalline phase increases with the decrease of temperature in presence of F-atoms.
8 Conversely, the etching selectivity yielding the microcrystalline phase increases with temperature in
9 SiH_4 plasmas. This explains and enables the growth of fully $\mu\text{c-Si}$ films at low temperature by
10 SiF_4 -based plasmas. Thus, not a “strong etching”, but rather a “strong etching selectivity” at low
11 temperature is the key difference between the growth of $\mu\text{c-Si}$ films from SiF_4 and SiH_4 plasmas.
12
13
14
15
16
17
18

19 In the below, we will present and analyze consequences of these main peculiarities of
20 fluorine atoms in the deposition of microcrystalline silicon from $\text{SiF}_4\text{-H}_2\text{-He}$ plasmas.
21
22
23
24
25

26 4. From amorphous to microcrystalline silicon films exploiting SiF_4 -based plasmas

27
28 Following the work by Ovshinsky and Madan [46], nowadays there is no doubt that $\text{SiF}_4\text{-H}_2$
29 plasmas can yield a-Si:H:F films with improved or at least the same optical and electrical quality as
30 a-Si:H from $\text{SiH}_4\text{-H}_2$ plasmas. Although it is known that a reference dielectric function does not
31 exist for a-Si, since its optical properties are a function of the deposition methods and parameters, a
32 relative comparison of the a-Si dielectric functions can be used to infer quality of materials. The
33 dielectric function is a fingerprint of a-Si, and it is highly sensitive to the hydrogen content of a-
34 Si:H and even hydrogen bond configuration, to the band gap and voids fraction/density. Therefore,
35 in Fig. 6 we are comparing the imaginary part, ϵ_2 , of the dielectric function of various a-Si:H
36 measured by us on films deposited from $\text{SiH}_4\text{-H}_2$ in various laboratories worldwide. In the same
37 figure, the spectrum of a typical a-Si:H:F film deposited by us from $\text{SiF}_4\text{-H}_2$ PECVD is also shown.
38 Optical transitions in amorphous materials lack k-vector conservation; hence, optical functions of
39 amorphous materials do not have very sharp features. The dielectric function exhibiting the largest
40 ϵ_2 at its peak (~ 30) from Aspnes [78] from LP-CVD (no hydrogen in the film) is believed to be
41 most representative of a bulk dense sample. It has been shown to be an apparently limiting peak
42 value for a-Si, and its $\epsilon(E)$ has long been regarded as the “intrinsic” dielectric properties of a-Si.
43 Interestingly, ϵ_2 at its peak ~ 30 is also achieved for a-Si:H (10% H) from PECVD deposited from
44 Arun Madan (a reference sample was provided to our lab) and from $\text{SiH}_4\text{-H}_2$ in our laboratories; a
45 reduced broadening is measured for a-Si:H, although typically lower values at the ϵ_2 maximum are
46 measured for films from $\text{SiH}_4\text{-H}_2$. Noteworthy, also the a-Si:H:F film deposited from $\text{SiF}_4\text{-H}_2$ in our
47 labs shows ϵ_2 at its peak ~ 30 although with a higher optical gap due to the fluorine inclusion.
48
49
50
51
52
53
54
55
56
57
58
59
60

1
2
3 Various dielectric functions representative of the amorphous silicon quality state-of-the-art from
4 various labs are reported in Fig. 6. Here, it can be seen that the amplitude and broadening of the
5 dielectric function of a-Si:H:F films similar to that of a-Si:H and a-Si, indicating similar optical
6 quality.
7
8
9

10
11 It is well known that to promote the amorphous-to- microcrystalline phase transition during
12 the PECVD of silicon from SiH₄-H₂, hydrogen dilution plays an important role [73,79,80].
13 Furthermore, the phase diagram proposed by Collins and his coworkers [81] indicates:
14

15
16 - the presence of an initial hydrogen-rich amorphous incubation layer, whose thickness decreases
17 with the increase in H₂ dilution, as also observed by many other groups [82].
18

19
20 - the existence of a crystallization dynamics, i.e., the increase in crystallinity with the increase in
21 film thickness [81];
22

23
24 - the dependence of cristallinity and the necessary H₂ dilution on plasma power, pressure, substrate
25 and temperature; specifically, the lower the deposition temperature, the higher the H₂ dilution to
26 have the amorphous-to-microcrystalline phase transition [83].
27

28
29 Therefore, H₂ dilution of SiH₄ poses some intrinsic limits to technological issues and objectives
30 such as deposition of fully crystalline films at low deposition temperature on plastic/polymer
31 flexible substrates. Furthermore, we have also to consider that the larger the H₂ dilution, the lower
32 the deposition rate (e.g. see Fig. 7). Those limitations have driven research on deposition of
33 microcrystalline silicon using approaches eliminating [27-34] or limiting [9,10] H₂ dilution.
34
35

36
37 Among the various approaches, we demonstrated that SiF₄-H₂-He r.f. PECVD is a valuable process
38 for the deposition of microcrystalline very thin films (thickness < 100 nm) at low temperatures
39 (<100°C), as shown in Fig. 7, also on plastic substrates.
40

41
42 Peculiarities of μ c-Si films deposited by the SiF₄-H₂-He PECVD are the complete crystallinity, the
43 very low hydrogen content (~1%) as indicated by FTIR measurements, the absence of any
44
45
46
47
48
49
50
51

52
53
54
55
56
57 amorphous incubation layer at the early stage of the growth and the absence of any crystallization
58 dynamics, as indicated by both Raman spectroscopy (see in the below) and ellipsometry. The
59 reliability of the ellipsometric analysis was calibrated and tested on some representative samples
60 [59] to be applied routinely to non destructive ellipsometric analysis of all samples.

1
2
3 Helium (He) has been chosen as diluents since it is a way to reduce ion energy, to high-
4 density plasmas at reduced r.f power and to films with lower defect density and lower hydrogen
5 content, producing more stable materials [84,85]. Furthermore, Lucovsky et al. [9,10] demonstrated
6 that the use of He to promote excitation and dissociation of SiH₄ and H₂ promoted the deposition of
7 homogeneous μc-Si films with no detectable amorphous silicon transition region between the
8 substrate and the μc-Si film. Figure 8 summarizes the effect of He dilution for fixed SiF₄/H₂ ratios.
9 The figure shows that for SiF₄-H₂-He plasmas, He dilution has an important effect and He is needed
10 to promote crystallinity. Specifically, an increase in the film crystallinity is observed with the
11 increase of He-dilution. Films with [H]<1% and a microvoids volume fraction of 5-10% are
12 obtained, indicating a release of hydrogen from the silicon network and an increase of film density
13 [38,40]. The increase in crystallinity accompanies with a decrease of the net deposition rate as a
14 consequence of a more effective etching of the amorphous phase with respect to the
15 microcrystalline phase [38]. Interestingly, the increase in microcrystallinity and density is achieved
16 for SiF₄-H₂-He plasmas at a low specific power $W/\Phi(\text{SiF}_4)\sim 1.5$, (defined as the effective plasma
17 power, W, per flux unit of the silicon precursor, Φ) and an increase in the $W/\Phi(\text{SiF}_4)$ parameter is
18 not needed, since it results in a decrease of crystallinity as shown in Fig. 9a. Conversely, high
19 values of $W/\Phi(\text{SiH}_4)$ are required to sustain crystallinity in SiH₄-H₂-He plasmas as shown in Fig.
20 9b. This effect of He in the SiF₄-H₂ plasmas can be explained by considering that an increase in the
21 ratio of the etching specie F-atoms to the SiF_x growth precursors is found by optical emission
22 spectroscopy (details are in ref. 38) sustaining the etching/deposition competition that favors the
23 crystalline phase formation.

24
25
26
27
28
29
30
31
32
33
34
35
36
37
38
39
40
41
42 As for the temperature effect on film microcrystallinity for films deposited from SiF₄, Fig. 10
43 shows the SE spectra of the imaginary part, $\langle \epsilon_2 \rangle$, of the pseudodielectric function of about 60 nm
44 and 100 nm thick μc-Si:H:F deposited on polyimide at various temperatures in the range 60–180°C.
45 The volume fractions of the microcrystalline (μc-), amorphous (a-) and voids phases constituting
46 the bulk of films, as derived from the BEMA modeling of the spectra, are also reported in the inset.
47 Interestingly, the a-Si phase decreases with decreasing temperature leading to an increase in the
48 voids volume fraction from 10% to 20% at very low temperatures.

49
50
51
52
53
54
55
56
57
58
59
60
Another characteristic of SiF₄-H₂-He plasmas about crystallization dynamics can be inferred by the
analysis of film microstructure as a function of film thickness. Figure 11 shows the $\langle \epsilon_2 \rangle$ spectra of
μc-Si:H:F films with different thickness deposited on both glass and polyimide. The small decrease
of the experimental SE spectra as a function of thickness can be ascribed to an increase of surface
roughness with thickness as corroborated by AFM data also reported in the same figure. A three-

layer model provided the best fit to spectra for glass samples, which consisted of a microcrystalline film (bottom layer), a less dense top-layer and the outmost surface roughness layer. For samples on polyimide, the best-fit to spectra was achieved by a two-layer model that consisted of the microcrystalline films and the top layer representing the growth zone and surface roughness. The fraction of the amorphous phase present in the top layer for the films on polyimide is consistent with the lower roughness also detected by AFM. For films on polyimide, less packed grains and, hence, less density film can be inferred from the presence of the 14-18% voids in the film, which might be related to the different initial nucleation density on the two substrates with different roughness. Furthermore, in this regime of fully microcrystalline films, without any amorphous component, the grain size increases with the increase in film thickness, as determined from XRD. From these best-fit SE models, corroborated by XRD and Raman measurements as shown in Fig. 12, it can be inferred that no amorphous interface is found by for the present films whatever the substrate. Figure 12 shows a typical Raman spectrum obtained for several microcrystalline samples on glass; the spectrum can be convolved with a narrow feature centred at 517 cm^{-1} with a full width half maximum (FWHM) of approximately $10\text{--}12\text{ cm}^{-1}$ due to a crystalline phase and a broad peak at $505\text{--}510\text{ cm}^{-1}$ with a FWHM = $25\text{--}29\text{ cm}^{-1}$ which is ascribable to small crystallites and/or grain boundaries. No appreciable amorphous component can be discerned at 480 cm^{-1} .

5. The substrate-film interface: the SiF_4 substrate pre-treatment for suppressing the incubation amorphous layer

Typically, a thin amorphous layer is formed at the substrate/film interface during deposition from $\text{SiH}_4\text{-H}_2$ plasmas. Therefore, many attempts have been made to improve crystallinity during the early stage of growth using fluorinated plasmas, e.g. $\text{SiF}_4\text{-H}_2$ plasmas [86,87] and $\text{CF}_4\text{-He}$ plasmas [88]. Film structure, including grain size and orientation, and crystalline fraction, can be controlled even at the early stage of growth by pre-treatments and modification of the substrate surface. In the below, we examine the use of $\text{SiF}_4\text{-He}$ plasmas for substrate pre-treatment in order to improve thin layers as seeds for subsequent $\mu\text{c-Si}$ deposition. The $\text{SiF}_4/\text{He}=20/45$ sccm plasma substrate pre-treatment was run at 20 Watt and 0.3 Torr.

A real time observation of the growth kinetics by laser reflectance interferometry (LRI) from both $\text{SiH}_4\text{-}$ and $\text{SiF}_4\text{-}$ based plasmas has revealed the existence of a “crystallite nucleation time”, which is the time indicative of the crystallites nucleation and coalescence. Typical LRI profiles are shown in the inset of Fig. 13. The increase in the reflectance signal is due to the optical contrast between the refractive index of the substrate and the refractive index of the forming silicon layer. Arrows in the inset indicate the onset of the nucleation process. The accurate determination of the nucleation point

1
2
3 depending on the substrate and deposition conditions has been measured by the first derivative of
4 the normalized reflectance curves: the time corresponding to the first derivative value of $2 \times 10^{-4} \text{ s}^{-1}$
5 of the normalized reflectance profiles identifies the nucleation onset. An investigation of the
6 dependence of the “crystallite nucleation time” on plasma substrate pre-treatments, i.e., H_2 and
7 $\text{SiF}_4\text{-He}$, on deposition plasmas, i.e., $\text{SiH}_4\text{-H}_2$ and $\text{SiF}_4\text{-H}_2$, and on substrates (including Corning
8 glass, c-Si and a flexible substrate such as the polyimide) has revealed that the $\text{SiF}_4\text{-He}$ pre-
9 treatment of substrates results in a longer nucleation time than the H_2 pre-treatment, as summarized
10 in Fig. 13. The different nucleation time indicates a different nucleation of silicon crystallites
11 depending on the substrate plasma pre-treatment, as also supported by the AFM data reported in the
12 same Fig. 13). In particular, the $\text{SiF}_4\text{-He}$ pre-treatment results in a longer nucleation time, with a
13 higher density and larger crystallites seeds on all substrates. Factors to be considered for explaining
14 the observed effect for SiF_4 substrate pre-treatment are: (i) the better cleaning (removal of native
15 oxide and contaminant) and lower substrate surface roughness achieved by the $\text{SiF}_4\text{-He}$ pre-
16 treatment; (ii) the surface passivation by atomic fluorine produced by the $\text{SiF}_4\text{-He}$ plasma (fluorine
17 on the surface has been detected by X-ray photoelectron spectroscopy), which inhibits random
18 nucleation of small nuclei; (iii) the deposition of $\mu\text{-Si}$ by chemical transport [89] from silicon
19 deposited on reactor walls.
20
21
22
23
24
25
26
27
28
29
30
31
32
33

34 The impact of the $\text{SiF}_4\text{-He}$ substrate pre-treatment on aiding microcrystallite nucleation and
35 growth also when using for the growth a SiH_4 -based plasma is reported in Fig. 14. Figure 14 shows
36 the SE spectra of the imaginary part, $\langle \epsilon_2 \rangle$, of the pseudodielectric function of $\mu\text{-Si}$ films with
37 different thickness deposited using $\text{SiH}_4\text{-H}_2$ plasmas at 120°C on SiF_4 pre-treated polyimide. The
38 microcrystallinity of the samples, even for a film as thin as $\sim 350\text{\AA}$, can be inferred by the presence
39 in the SE spectra of the sharp E_1 and E_2 critical points. Fit to spectra has been achieved by a three-
40 layer model that consist of the initial nucleation layer, which is a mixture of fine grains (p-Si-f) and
41 voids, the film where the voids density decreases because of the increase in grain size as also
42 indicated by the AFM images, and the top surface roughness layer, as indicated in the figure. It is
43 interesting noting that the SiF_4 pre-treatment of polyimide results in direct nucleation and growth of
44 fully microcrystalline films on polyimide without any amorphous interface layer even using highly
45 H_2 -diluted SiH_4 . Furthermore, the corresponding AFM data, also reported in the same figure, show
46 an increase of the average grain size with film thickness. A similar behavior, i.e., fully
47 microcrystalline material without interface layer at the substrate and with a grain size that increases
48 with film thickness, applies also for films deposited by $\text{SiH}_4\text{-H}_2$ plasmas on SiF_4 pre-treated glass
49 [90,91]. Therefore, when the $\text{SiF}_4\text{-He}$ substrate pre-treatment is applied, direct seeding of
50 crystallites without any amorphous tissue promotes fully microcrystalline films independently of
51
52
53
54
55
56
57
58
59
60

1
2
3
4
5
6
7
8
9
10
11
12
13
14
15
16
17
18
19
20
21
22
23
24
25
26
27
28
29
30
31
32
33
34
35
36
37
38
39
40
41
42
43
44
45
46
47
48
49
50
51
52
53
54
55
56
57
58
59
60

thickness. In this case, dynamics only concerns grain size increase according to the cone model proposed by Branz and his group [92].

6. Summary

The peculiarities of the use of the SiF_4 precursor in the deposition of a-Si:H:F and of $\mu\text{c-Si:H:F}$ by r.f. PECVD have been presented and discussed. The primary conclusions can be summarized as follow:

- the growth of silicon films both amorphous and micro-crystalline from SiF_4 plasmas requires hydrogen atoms;
- the concomitant presence of both etchants fluorine and hydrogen atoms allows the amorphous-to-microcrystalline transition to occur at low H_2 dilution of $\text{SiF}_4\text{-H}_2$ plasmas. The microcrystallinity results from the deposition/etching competition;
- fluorine atoms, acting as heterogeneous scavenger of hydrogen atoms, results in lower hydrogen content into the films and more dense and stable microstructures;
- $\text{SiF}_4\text{-H}_2$ plasmas allow the growth of microcrystalline materials reducing any amorphous incubation layer at the substrate/film interface;
- $\text{SiF}_4\text{-H}_2$ plasmas allow the growth of micro-crystalline films at low temperatures ($T < 100^\circ\text{C}$) also on flexible substrates.
- the He dilution of $\text{SiF}_4\text{-H}_2$ plasmas aids and promotes crystallization;
- $\text{SiF}_4\text{-He}$ plasmas are also worthy as substrate pre-treatment in order to promotes crystallites seeds for the subsequent $\mu\text{c-Si}$ deposition.

Acknowledgements

The authors are grateful to Mr Alberto Sacchetti at IMIP-CNR for the technical assistance in performing the PECVD deposition experiments.

The 7th FP European Project NanoCharM (Multifunctional NanoMaterials Characterization exploiting Ellipsometry and Polarimetry) (NMP3-CA-2007-218570) is also acknowledged.

For Peer Review Only

1
2
3
4
5
6
7
8
9
10
11
12
13
14
15
16
17
18
19
20
21
22
23
24
25
26
27
28
29
30
31
32
33
34
35
36
37
38
39
40
41
42
43
44
45
46
47
48
49
50
51
52
53
54
55
56
57
58
59
60

References

- [1] D.E. Carlson, C.R. Wronski, Appl. Phys. Lett. 28 (1976) p.671.
- [2] M.H. Brodsky, M.A. Frisch, J.F. Ziegler, W.A. Lanford, Appl. Phys. Lett. 30 (1977) p.561.
- [3] D.L. Staebler, C.R. Wronski, Appl. Phys. Lett. 31 (1977) p.292.
- [4] G. Lucovsky, H. Yang, J. Non-Cryst. Solids 230 (1998)p. 281
- [5] W.E. Spear, G. Willeke, P.G. Lecomber, A.G. Fitzegerald, J. de Physique 42 (1981) p.257.
- [6] P.G. Lecomber, G. Willeke, W.E. Spear, J. Non-Cryst. Solids 59-60 (1983) p.795.
- [7] Z. Iqbal, F.A. Sarott, S. Veprek, J. Phys. C, 16 (1983) p.2005.
- [8] K. Tanaka, A. Matsuda, Mater.Sci. Rep. 2 (1987) p.139.
- [9] G. Lucovsky, C. Wang, R.J. Nemanich, M.J. Williams, Solar Cells 30 (1991) p.419.
- [10] C.Wang, M.J. Williams, G. Lucovsky, J. Vac. Sci. Technol. A 9 (1991) p.444.
- [11] H. Morikawa, T. Itagaki, K. Kawabata, T. Ishihara, K. Sato, H. Namizaki, Solar Energy Materials 23 (1991) p.199.
- [12] M. Kaneiwa, S. Okamoto, I. Yamasaki, M. Nishida, T. Nammori, Solar Energy Materials an Solar Cells 34 (1994) p.183.
- [13] J. Meier, R. Flückiger, H. Keppner, A. Shah, Appl. Phys. Lett. 65 (1994) p.860.
- [14] D.V. Tsu, B.S. Chao, S.R. Ovshinsky, S. Guha, J. Yang, Appl. Phys. Lett. 71 (1997) p.1317.
- [15] J. Koh, A. S. Ferlauto, P. I. Rovira, C. R. Wronski, R. W. Collins, Appl. Phys. Lett. 75 (1999) p.2286.
- [16] J. Koh, Y. Lee, H. Fujiwara, C. R.Wronski, R.W. Collins, Appl. Phys. Lett. 73 (1998) p.1526.
- [17] S. Guha, J. Yang, D. L. Williamson, Y. Lubianiker, J. D. Cohen, A. H. Mahan, Appl. Phys. Lett. 74 (1999) p.1860.
- [18] S.Y. Myong, S.W. Kwon, K.S. Lim, M. Kondo, M. Konagai, Appl. Phys. Lett. 88 (2006) 083118.
- [19] S.Y. Myong, S.W. Kwon, M. Kondo, M. Konagai, K.S. Lim, Semicond. Sci. Technol. 21 (2006) p.L11.
- [20] A. Mossad Ali, T. Inokuma, S. Hasegawa, Applied Surface Science 253 (2006) p. 1198
- [21] R. Huang, X. Lin, Y. Yu, K. Lin, Z. Zhu, J. Wei, K. Chen, J. Phys. D: Appl. Phys. 39 (2006) p.4423.
- [22] D. V. Tsu, B. S. Chao, S. R. Ovshinsky, S. Guha, J. Yang, Appl. Phys. Lett. 71 (1997) p.1317.
- [23] T. Kamei, P. Stradins, A. Matsuda, Appl. Phys. Lett. 74 (1999) p.1707.
- [24] M. Isomura, M. Kondo, A. Matsuda, Japan. J. Appl. Phys. 39 (2000) p.3339.
- [25] A.M. Ali, S. Hasegawa, Thin Solid Films 437 (2003) p.68.

- 1
2
3 [26] D. Han, K. Wang, J.M. Owens, L. Gedvilas, B. Nelson, H. Habuchi, M. Tanaka, J. Appl. Phys.
4 93 (2003) p.3776.
5
6 [27] M. Isomura, M. Kondo, A. Matsuda, Jpn. J. Appl. Phys. 39 (2000) p.4721.
7
8 [28] Y. Hishikawa, S. Tsuge, K. Wakisaka, Y. Kuwano, J. Appl. Phys. 73 (1993) p.4227.
9
10 [29] M.N. van den Donker, B. Rech, F. Finger, W.M.M. Kessels, M.C.M. van de Sanden Appl.
11 Phys. Lett. 87 (2005) 263503.
12
13 [30] B. Strahm, A.A. Howling, L. Sansonnens, Ch. Hollenstein, U. Kroll, J. Meier, Ch. Ellert, L.
14 Feitknecht, C. Ballif, Sol. Energy Mat. Sol. Cells 91 (2007) p.495.
15
16 [31] T. Roschek, B. Rech, J. Muller, R. Schmitz, H. Wagner, Thin Solid Films 451-452 (2004)
17 p.466.
18
19 [32] L. Feitknecht, J. Meier, P. Torres, J. Zurcher, A. Shah, Sol. Energy Mat. Sol. Cells 74 (2002)
20 p.539.
21
22 [33] S.B. Li, Z.M. Wu, Y.D. Jiang, J.S. Yu, W. Li, N.M. Liao, J. Phys. D. 41 (2008) 105207.
23
24 [34] H.B. Kim, H.C. Lee, K.N. Kim, G.Y. Yeom, J. Vac. Sci. Technol. A 26 (2008) p.842.
25
26 [35] T. Kamiya, K. Nakahata, T. Sameshima, T. Watanabe, T. Mouri, I. Shimizu, J. Appl. Phys. 88
27 (2000) p.3310.
28
29 [36] T. Nishimoto, T. Takagi, M. Kondo, A. Matsuda, Solar Energy Materials & Solar Cells 66
30 (2001) p.179.
31
32 [37] M. Syed, T. Inokuma, Y. Kurata, S. Hasegawa, Jpn. J. Appl. Phys. 36 (1997) p.6625.
33
34 [38] G. Cicala, P. Capezzuto, G. Bruno, J. Vac. Sci. Technol. A 19 (2001) p.515.
35
36 [39] M.M. Giangregorio, M. Losurdo, A. Sacchetti, P. Capezzuto, G. Bruno, Thin Solid Films 511-
37 512, (2006) p.598
38
39 [40] M. Losurdo, M.M. Giangregorio, A. Grimaldi, P. Capezzuto, G. Bruno, Europ. Phys. J. Appl.
40 Phys. 26 (2004) p. 187.
41
42 [41] G. Bruno, P. Capezzuto, F. Cramarossa, R. d'Agostino, Thin Solid Films, 67 (1980) p.103.
43
44 [42] H. Shirai, Thin Solid Films, 457 (2004) p.90.
45
46 [43] Y. Li, Y. Ikeda, Y. Toyoshima, H. Shirai, Thin Solid Films 506– 507 (2006) p.38.
47
48 [44] J.A. Theil, G. **Lucovsky**, S.V.Hattangady, MRS Symp. Procced. 220 (1991) p.601.
49
50 [45] T. Saito, Y. Li, Y. Ikeda, H. Shirai, J. Non-Crys. Solids 352 (2006) p.1967.
51
52 [46] S.R. Ovshinsky, A. Madan, Nature, 276 (1978) p.482.
53
54 [47] C.H.L. Goodman, Nature, 279 (1979) p.349.
55
56 [48] G. Cicala, G. Bruno, P. Capezzuto J. Vac. Sci. Technol. A 16 (1998) p.2762.
57
58 [49] A. Madan, S.R. Ovshinsky, J. Non-Cryst. Solids 35-36 (1980) p.171.
59
60 [50] N. Shibata, S. Oda, I. Shimizu, Jpn. J. Appl. Phys. 26 (1987) p.L276.

1
2
3
4
5
6
7
8
9
10
11
12
13
14
15
16
17
18
19
20
21
22
23
24
25
26
27
28
29
30
31
32
33
34
35
36
37
38
39
40
41
42
43
44
45
46
47
48
49
50
51
52
53
54
55
56
57
58
59
60

- [51] Uesugi et al Jpn.J. Appl. Phys. 24 (1985) p.909.
- [52] T. Nishimoto, T. Takagi, M. Kondo, A. Matsuda, Solar Energy Materials & Solar Cells 66 (2001) p.179.
- [53] L.E. Mosley, M.A. Paesler, **G. Lucovsky**, et al. Solid State Comm. 53 (1985) p.513.
- [54] W.E. Spear, R.J. Loveland, A. Al-Sharbaty, J. Non-Cryst. Solids 15 (1974) p.410.
- [55] A.C. Hourd, D.L. Melville, W.E. Spear Phil. Mag. B 64 (1991) p. 533.
- [56] G. Cicala, M. Losurdo, P. Capezzuto, G. Bruno, Plasma Sources Sci. Technol. 1 (1992) p.156.
- [57] A. Haddad Adel, T. Inokuma, Y. Kurata, S. Hasegawa, Journal of Non-Crystalline Solids 351 (2005) p.2107.
- [58] G.E. Jellison, F.A. Modine, Appl. Phys. Lett. 69 (1996) p. 371 and p. 2137.
- [59] M. Losurdo, R. Rizzoli, C. Summonte, G. Cicala, P. Capezzuto, G. Bruno, J. Appl. Phys. 88 (2000) p. 2408.
- [60] G.E. Jellison, M.F. Chisholm, M. Gorbalkin, Appl. Phys. Lett. 62 (1993) p.3348.
- [61] A. Matsuda, K. Nomoto, Y. Takeuchi, A. Suzuki, A. Yuuki, J. Perrin, Surf. Sci. 227 (1990) p.50.
- [62] [G. Lucovsky, B.N. Davidson, G.N. Parsons, et al, J. Non-Crys. Solids 114 (1989) p.154
- [63] G.N. Parsons, C. Wang, M.J. Williams, G. Lucovsky, et al. J. Non-Crys. Solids 114 (1989) p.178
- [64] A. Matsuda, J. Non-Cryst. Solids 59-60 (1983) p.767.
- [65] A. Matsuda, J. Non-Cryst. Solids 338-340 (2004) p.1.
- [66] G. Lucovsky, J. Non-Crys. Solids 141 (1992) p.241.
- [67] G.N. Pearson, C. Wang, M.J. Williams, G. Lucovsky et al. Appl. Phys. Lett. 56 (1990) p.1895.
- [68] G. Lucovsky, G.N. Parsons, C. Wang et al. Solar Cells 27 (1989) p.121.
- [69] G. Bruno, P. Capezzuto, G. Cicala, J. Appl. Phys. 69 (1991) p.7256.
- [70] K. Nakahata, K. Ro, A. Suemasu, T. Kamiya, C.M. Fortmann, I. Shimizu, Jpn. J. Appl. Phys. 39 (2000) p.3294.
- [71] B. Lee, L.J. Quinn, P.T. Baine, S.J.N. Mitchell, B.M. Armstrong, H.S. Gamble, Thin Solid Films 337 (1999) p.55.
- [72] A. Matsuda, Thin Solid Films 337 (1999) p.1.
- [73] W. Futako, K. Yoshino, C.M. Fortmann, I. Shimizu, J. Appl. Phys. 85 (1999) p.812.
- [74] J.I. Woo, H.J. Lim and J. Jang, Appl. Phys. Lett. 65 (1994) p.1644.
- [75] T. Kamiya, A. Suemasu, T. Watanabe, T. Sameshima, I. Shimizu, Appl. Phys. A 73 (2001) p.151.
- [76] A. Haddad Adel, T. Inokuma, Y. Kurata, S. Hasegawa, Surface Science 600 (2006) p.4418.

- 1
2
3 [77] D. Humbird, D. B. Graves, J. Appl. Phys., 96 (2004) p.792.
4
5 [78] D. E. Aspnes, A. A. Studna, E. Kinsbron, Phys. Rev. B 29 (1984) p.768.
6
7 [79] K. Tanaka, A. Matsuda, Mater.Sci. Rep. 2 (1987) p.139]
8
9 [80] H. Fujiwara, M. Kondo, A. Matsuda, Surf. Sci. 497 (2002) p.333.
10
11 [81] R.W. Collins, A.S. Ferlauto, G.M. Ferreira, C. Chen, J. Koh, R.J. Koval, Y. Lee, J.M. Pearce,
12 C.R. Wronski, Solar Energy Materials & Solar Cells 78 (2003) p.143.
13
14 [82] M. Birkholz, B. Selle, W. Fuhs, S. Christiansen, H.P. Strunk, R. Reich, Phys. Rev. B 64 (2001)
15 p.085402 and references therein.
16
17 [83] P. Alpuim, V. Chu, J.P. Conde, J. Appl. Phys. 86 (1999) p.3812.
18
19 [84] S. Tchakarov, D. Das, O. Saadane, A.V. Kharchenko, V. Suendo, F. Kail, P.Roca I Cabarrocas,
20 J. Non-Cryst. Solids 338-340 (2004) p.668.
21
22 [85] J.C. Knights, R.A. Lujian, M.P. Rosenblum, R.A. Street, D.K. Bieglesen, J.A. Reimer, Appl.
23 Phys. Lett. 38 (1981) p.331.
24
25 [86] T. Kamiya, K. Ro, C.M. Fortmann, I. Shimizu, Jpn. J. Appl. Phys. 38 (1999) p.5762.
26
27 [87] D. Matsuura, T. Kamiya, C.M. Fortmann, I. Shimizu, Solar Energy Materials & Solar Cells 66
28 (2001) p.305.
29
30 [88] M. Syed, T. Inokuma, Y. Kurata, S. Hasegawa, Jpn. J. Appl. Phys. 41 (2002) p.263.
31
32 [89] S. Veprek, Z. Iqbal, H.R. Oswal, A.P. Weeb, J. Phys. C. Solid State Phys. 14 (1981) p.295.
33
34 [90] M.M. Giangregorio, M. Losurdo, A. Sacchetti, P. Capezzuto, F. Giorgis, G. Bruno, Appl. Surf.
35 Sci. 253 (2006) p.287.
36
37 [91] M. Losurdo, M.M. Giangregorio, A. Sacchetti, P. Capezzuto, G. Bruno, J. Carabe, J.J. Gandia,
38 L. Urbina, J. Non.Cryst. solids 352 (2006) p.906.
39
40 [92] C.W. Teplin, C.S. Jiang, P. Stradins, H.M. Branz, Appl. Phys. Lett. 92 (2008) p.093114.
41
42
43
44
45
46
47
48
49
50
51
52
53
54
55
56
57
58
59
60

Figure Captions

Figure 1. Scheme representing the silicon *deposition* (activated by SiF_x radicals and hydrogen atoms) and the silicon *etching* (operated by fluorine atoms) processes with the corresponding kinetic equations for the deposition rate, r_D , and etching rate, r_E . The scheme has been drawn on the basis of a previous model from Matsuda [65]. The formation of the microcrystalline phase results from the deposition/etching competition: a much higher deposition rate than etching rate mainly yields the amorphous phase, whereas a deposition rate slightly higher than the etching rate results in the amorphous-to-microcrystalline phase transition.

Figure 2. Dependence of the crystalline (f_c), amorphous (f_a) and voids volume fractions (as determined by the analysis of ellipsometric spectra) of 100nm thick films deposited on Corning glass 7059 as a function of the SiF_4/H_2 ratio at a temperature of 250°C.

Figure 3. Ellipsometric spectra and best-fit models of $\mu\text{c-Si:H:F}$ and $\mu\text{c-Si:H}$ films deposited by $\text{SiF}_4/\text{H}_2=2$ (dilution of 60 % in He) and $\text{SiH}_4/\text{H}_2=0.017$ plasmas, respectively, at 180°C on Corning Glass. The corresponding $1\mu\text{m}\times 1\mu\text{m}$ AFM images and rms values (root mean square surface roughness) are also shown indicating a lower surface roughness for the $\mu\text{c-Si:H:F}$ film.

Figure 4. Like-Arrhenius plot for the etching rate of $\mu\text{c-Si}$ and a-Si films by fluorine atoms (F-atoms) and hydrogen atoms (H-atoms).

For the a-Si:H, deposition conditions were: $\text{SiH}_4/\text{H}_2=2\text{sccm}/18\text{sccm}$, pressure = 0.3 Torr, r.f. power = 10 Watt, T = 200 °C, thickness = 1 μm

The $\mu\text{c-Si}$ were deposited by $\text{SiF}_4/\text{H}_2/\text{He} = 20/10/45\text{sccm}$ at 100°C, 0.3 Torr and 20 Watt.

For the etching experiments of a-Si and $\mu\text{c-Si}$ films by atomic hydrogen and fluorine H_2 and NF_3 plasmas were used, respectively. Etching plasmas were operated at a flux of 10 sccm, a r.f. power of 5 Watt, a pressure of 0.003 Torr, while the surface temperature was varied from room temperature to 350 °C.

Figure 5. Etching selectivity parameter, defined as the ratio between the etching rate of the a-Si and $\mu\text{c-Si}$, $r_{\text{a-Si}}/r_{\mu\text{c-Si}}$, vs. temperature in F-atoms and H-atoms containing plasmas. The

1
2
3 diagram shows that at $T > 100^\circ\text{C}$ hydrogenated plasmas (SiH_4) favor deposition of $\mu\text{c-Si}$
4 films, while fluorinated plasmas (SiF_4) favor a-Si films formation; at $T < 100^\circ\text{C}$, the
5 reverse applies, i.e., fluorinated plasmas (SiF_4) favor deposition of $\mu\text{c-Si}$ films, while
6 hydrogenated plasmas (SiH_4) favor the a-Si phase.
7
8
9

10
11
12 **Figure 6.** Dielectric function (blue lines) of various a-Si:H films deposited by $\text{SiH}_4\text{-H}_2$ PECVD in
13 different laboratories; the a-Si:H_{Bari}(from our lab) and from a reference a-Si:H_{Madan}
14 provided by Arun Madan well compare with the “reference intrinsic” a-Si:Asp dielectric
15 function from Aspnes in ref. [78] (black line). The dielectric function (red line) for a
16 typical a-Si:H:F film deposited from $\text{SiF}_4\text{-H}_2$ in our lab at $T = 250^\circ\text{C}$ is also shown for
17 comparison.
18
19
20
21
22
23

24
25 **Figure 7.** Dependence on the deposition temperature of the deposition rate (dashed line,) and
26 crystallinity (continuous line) for films deposited by $\text{SiF}_4/\text{H}_2=2$ (dilution of 60% in He)
27 plasmas (red lines, square symbols). Data for deposition from $\text{SiH}_4\text{-H}_2$ plasmas at a
28 dilution of 90% (●,○) and 95% (▲,▽) in H_2 from ref. [83] are also shown for
29 comparison, and despite the low number of $\text{SiH}_4\text{-H}_2$ points, lines are to draw eye to the
30 trend. (Thickness of the deposited films is approximately 200nm)
31
32
33
34
35
36

37 **Figure 8.** Dependence on He dilution of the crystalline and voids volume fractions (as determined
38 by the analysis of ellipsometric spectra) for 100nm thick films deposited on Corning
39 glass from $\text{SiF}_4\text{-H}_2$ $\text{SiF}_4/\text{H}_2=4$; indicative points also for $\text{SiF}_4/\text{H}_2=2$ and 5 are also shown.
40
41
42 Thickness of the deposited films is in the range 150-200nm.
43
44
45

46 **Figure 9.** Crystalline (●), amorphous (■) and voids (○) volume fractions vs rf power for films
47 deposited from (a) $\text{SiF}_4\text{-H}_2$ plasmas ($\text{SiF}_4/\text{H}_2=4$, dilution of 60% in He) and (b) $\text{SiH}_4\text{-H}_2$
48 plasmas with $C(\text{SiH}_4)=2\%$.
49
50
51
52

53 **Figure 10.** Experimental ellipsometric spectra of the imaginary part, $\langle \varepsilon_2 \rangle$, of the pseudodielectric
54 function of $\mu\text{c-Si}$ film deposited on polyimide at various temperatures. The inset shows
55 the corresponding volume fractions of the microcrystalline ($\mu\text{c-}$), amorphous (a-) and
56 voids phases constituting the silicon films as derived by the BEMA analysis of SE
57 spectra.
58
59
60

1
2
3
4 **Figure 11.** Experimental SE spectra of the imaginary part, $\langle \epsilon_2 \rangle$, of the pseudodielectric function of
5 $\mu\text{c-Si}$ film with different thickness deposited from $\text{SiF}_4\text{-H}_2\text{-He}$ plasmas at 100°C on (a)
6 Corning glass and (b) polyimide. The best-fit ellipsometric models and the
7 corresponding $1\mu\text{m}\times 1\mu\text{m}$ AFM images with the surface roughness (RMS) values are
8 also shown. The E_1 and E_2 critical points, which are signature of the crystalline phase
9 are also indicated.

10
11
12
13
14
15
16 **Figure 12.** Raman spectrum of a typical microcrystalline sample deposited on glass_black line (it
17 corresponds to the SLV55 sample in Fig. 11) and on polyimide_red line (it corresponds
18 to the 414\AA thick film in Fig. 11).

19
20
21 The Raman spectra were acquired by a Renishaw spectrophotometer equipped with a
22 cooled CCD detector and a laser excitation at 514.5 nm in confocal-backscattering
23 configuration, focussing the beam with a power of 1 mW into a spot of $1\text{ }\mu\text{m}$ through a
24 X100 microscope objective.
25
26
27
28
29

30 **Figure 13.** Nucleation time of silicon deposition from $\text{SiH}_4\text{-H}_2$ and $\text{SiF}_4\text{-H}_2$ plasmas using the $\text{SiF}_4\text{-}$
31 He and the H_2 pre-treatment of polyimide, Corning glass 7059 and $\text{Si}(100)$ substrates.
32 The inset shows the laser reflectance interferometry (LRI) traces recorded during the
33 $\mu\text{c-Si}$ films deposition at 230°C on glass, putting in evidence the different nucleation
34 time depending on the substrate pre-treatment. The $1\mu\text{m}\times 1\mu\text{m}$ AFM images with the
35 corresponding rms values of the glass substrates after the H_2 and $\text{SiF}_4\text{-He}$ pre-treatment
36 and after the subsequent deposition of 20 nm of $\mu\text{c-Si}$ film are also shown.
37
38
39
40
41
42
43
44

45 **Figure 14.** SE spectra of the imaginary part, $\langle \epsilon_2 \rangle$, of the pseudodielectric function of $\mu\text{c-Si}$ films
46 with different thickness deposited at 120°C on SiF_4 pre-treated polyimide using a $\text{SiH}_4\text{-}$
47 $\text{H}_2=0.5\text{-}30\text{ sccm}$ plasma at 0.3 torr and at a r.f. power density of 170mW/cm^2 . The best-
48 fit corresponding BEMA models showing the microstructure of films and the
49 corresponding $1\mu\text{m}\times 1\mu\text{m}$ AFM images with the surface roughness (RMS) values are
50 also reported. The E_1 and E_2 critical points, which are signature of the crystalline phase
51 are also indicated.
52
53
54
55
56
57
58
59
60

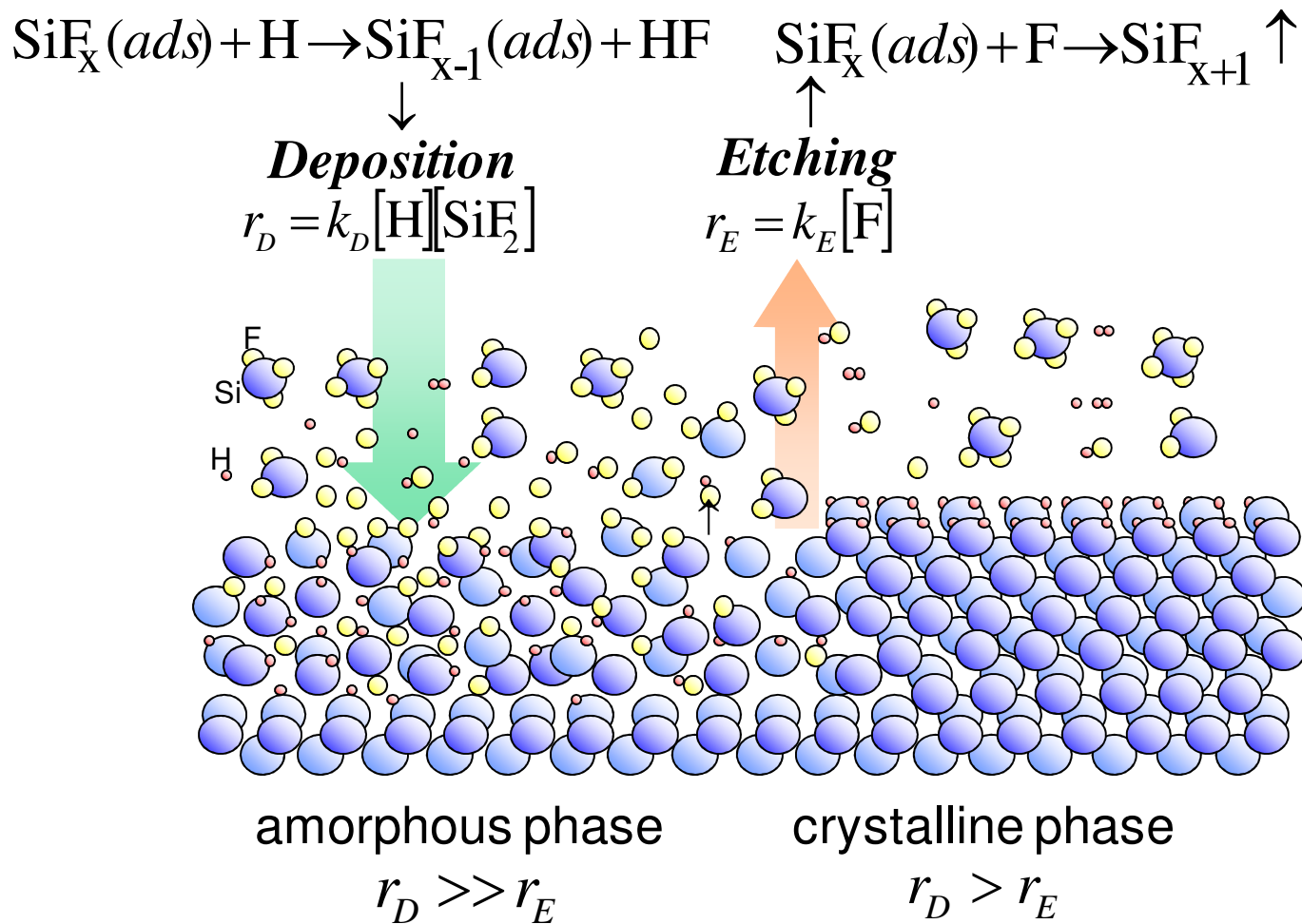


Figure 1

1
2
3
4
5
6
7
8
9
10
11
12
13
14
15
16
17
18
19
20
21
22
23
24
25
26
27
28
29
30
31
32
33
34
35
36
37
38
39
40
41
42
43
44
45
46
47
48
49
50
51
52
53
54
55
56
57
58
59
60

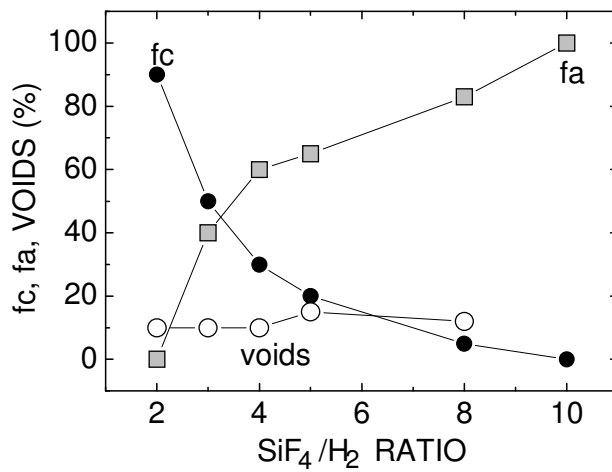


Figure 2

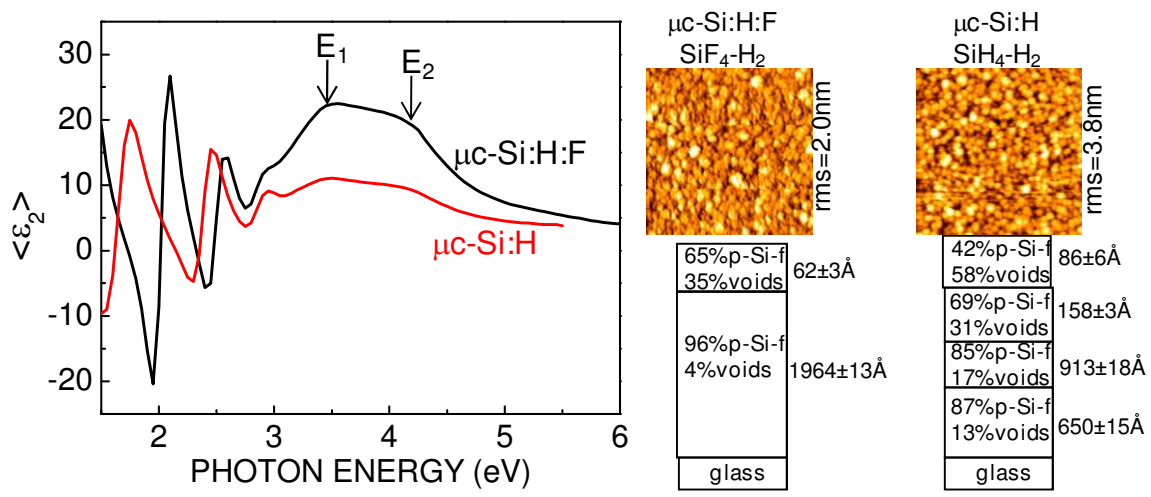


Figure 3

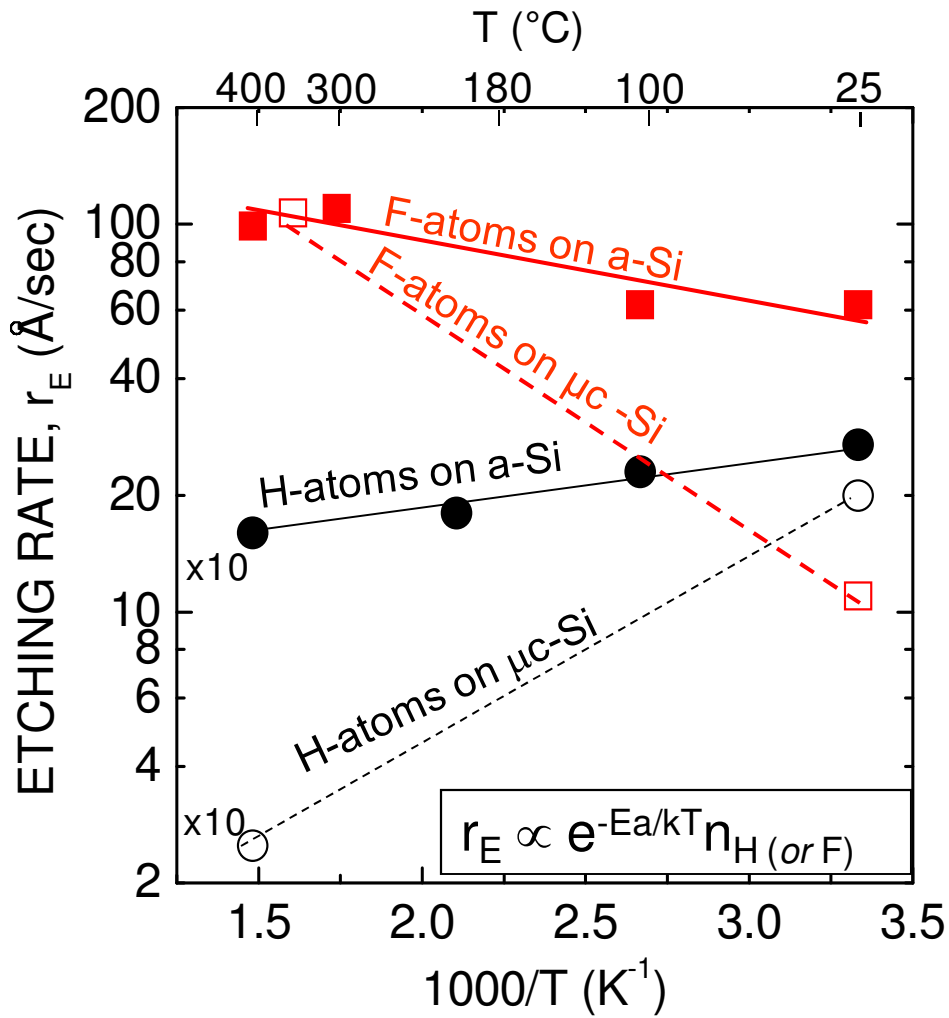


Figure 4
Figure 4

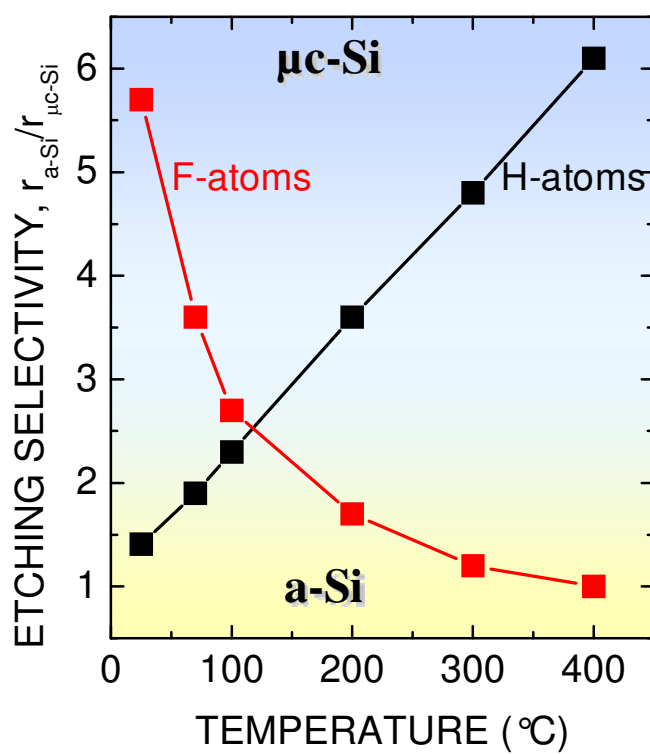


Figure 5

1
2
3
4
5
6
7
8
9
10
11
12
13
14
15
16
17
18
19
20
21
22
23
24
25
26
27
28
29
30
31
32
33
34
35
36
37
38
39
40
41
42
43
44
45
46
47
48
49
50
51
52
53
54
55
56
57
58
59
60

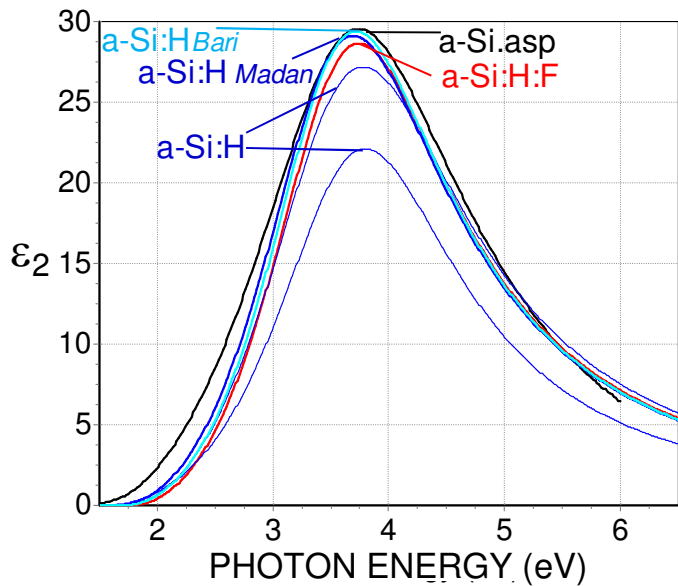


Figure 6

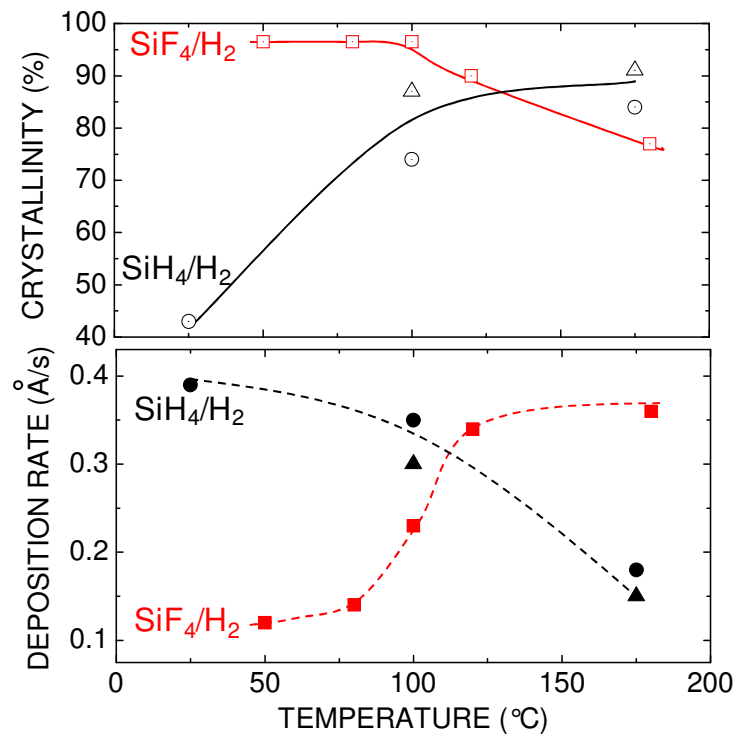


Figure 7

1
2
3
4
5
6
7
8
9
10
11
12
13
14
15
16
17
18
19
20
21
22
23
24
25
26
27
28
29
30
31
32
33
34
35
36
37
38
39
40
41
42
43
44
45
46
47
48
49
50
51
52
53
54
55
56
57
58
59
60

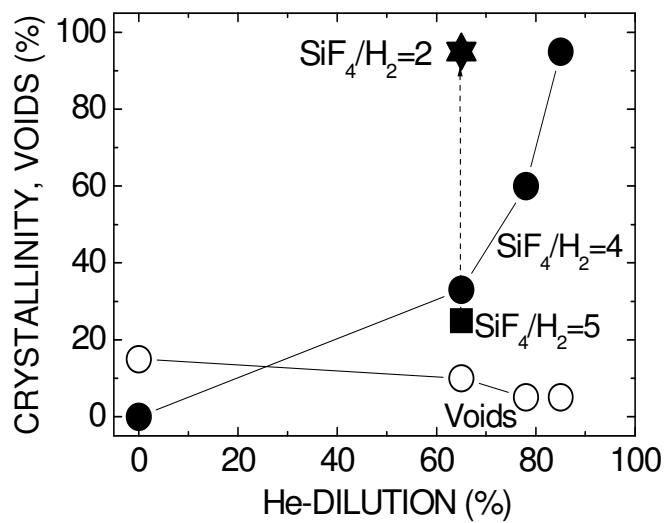


Figure 8

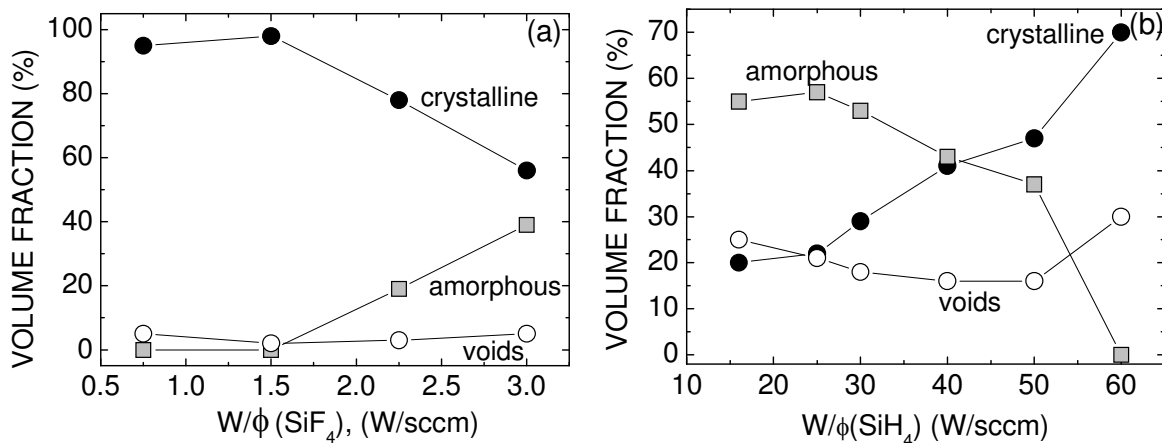


Figure 9

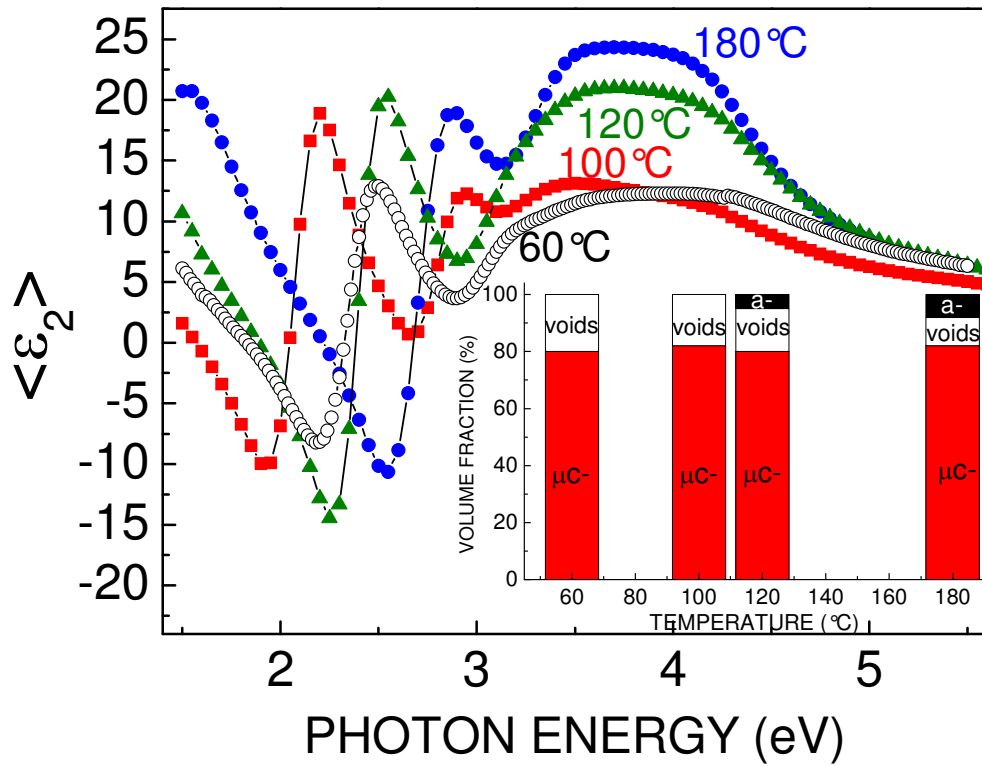


Figure 10

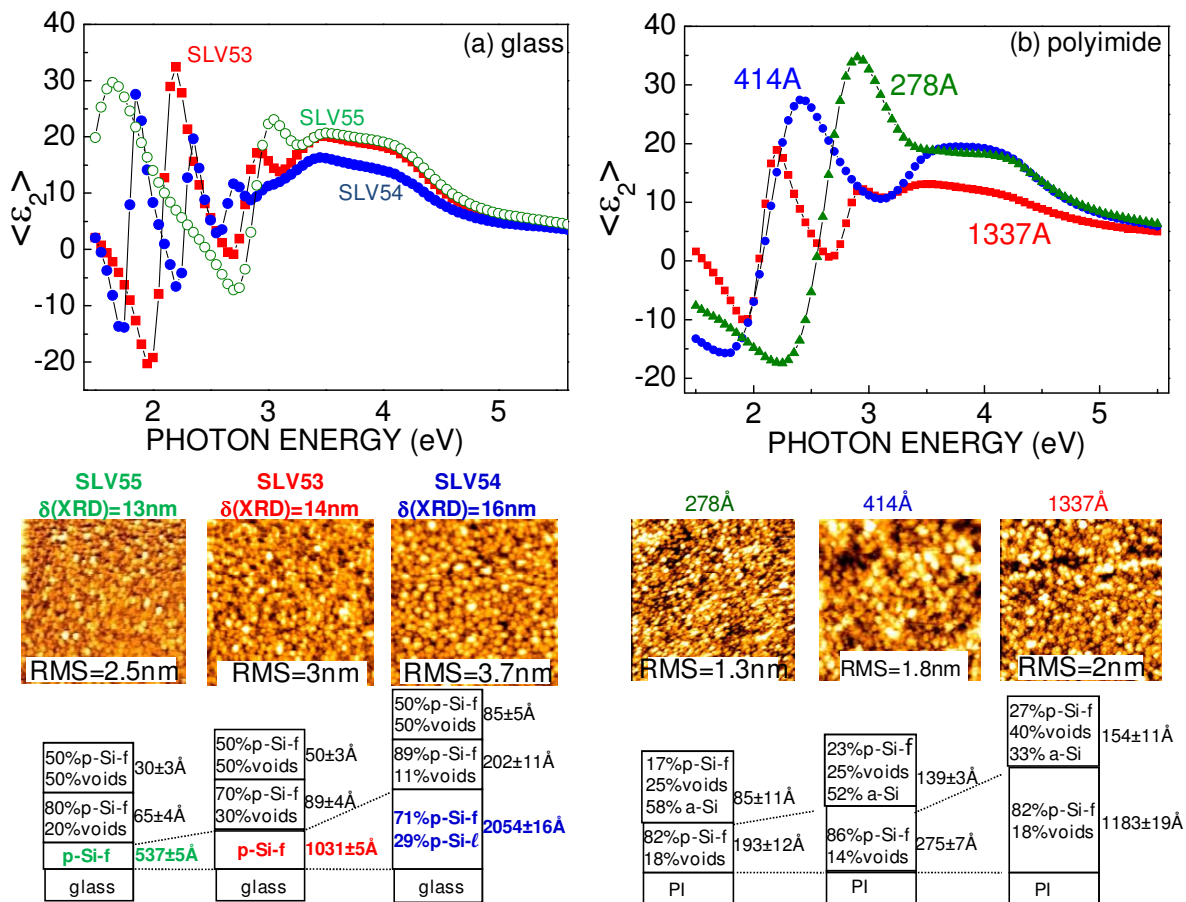


Figure 11

1
2
3
4
5
6
7
8
9
10
11
12
13
14
15
16
17
18
19
20
21
22
23
24
25
26
27
28
29
30
31
32
33
34
35
36
37
38
39
40
41
42
43
44
45
46
47
48
49
50
51
52
53
54
55
56
57
58
59
60

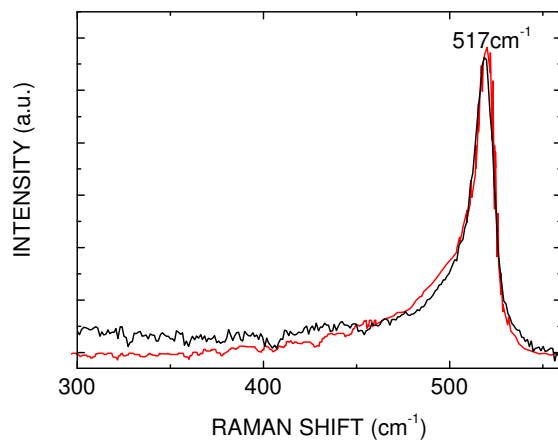


Figure 12

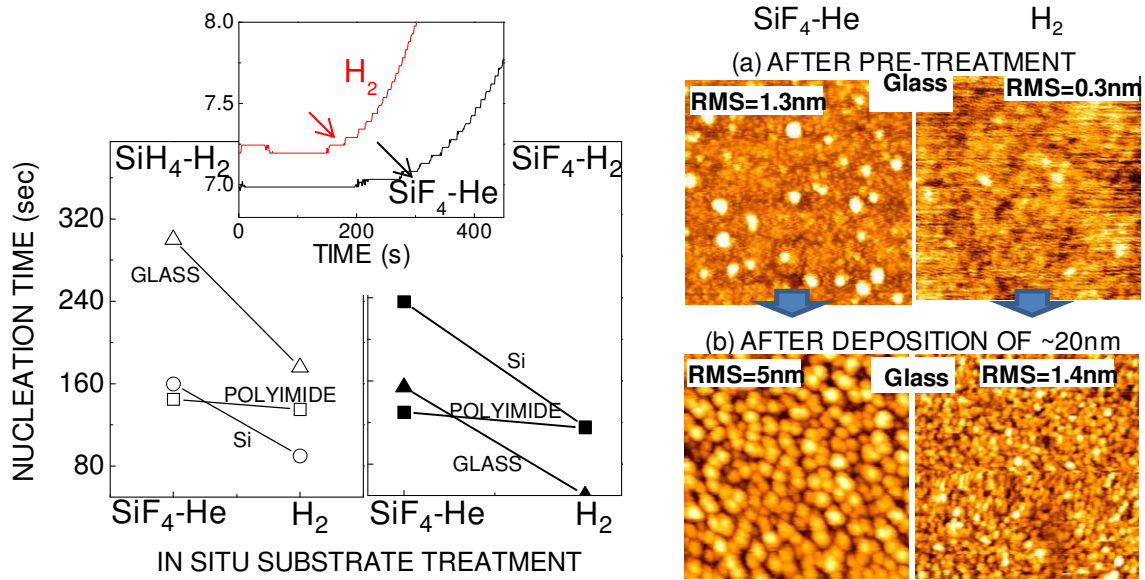


Figure 13

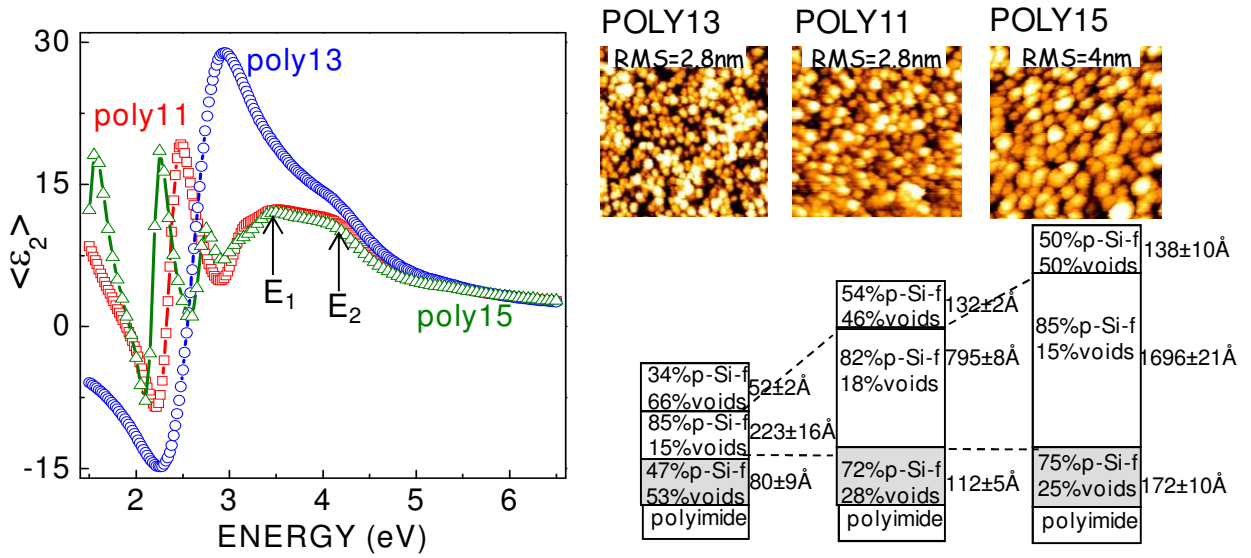


Figure 14